IJCTA, 8(4), 2015, pp. 1473-1482

Design Material of Coupled Inuctor For The Boost Converter in Solar Application

P. Muthukrishnan*, R. Dhanasekaran and C. Elavazhagan*****

Abstract: In the Modern world we are using many different renewable Energy systems. Each and every system are most probably the DC generating systems in this DC systems Power boosting is the major role which can be achieved by means of using different kinds of Boost converters. In this boosting operation many of the converters are working depends on the isolation transformers. The main drawback in this type of isolation transformers are leakage inductance due to the materials used in isolation transformers. Such kind of leakage inductance can be reduced by the modern transient coupled inductor phenomenon. This main focus of the Project is to design the coupled inductor. During the design of coupled inductor the main considerations are core material, Inductor material, dielectric materials. Core material design we are chosen here to reduce the electromagnetic leakages. Using materials such as Ferro cube 3C94, Ferro cube 3C81, Metglas 2605SA1 and its analysis have to done in this Paper

Keywords: Boost Converter, Core material design, Coupled Inductor, dielectric materials, High Voltage Gain, Inductor material, Load Capacitor.

1. INTRODUCTION

The construction of core material is the major process of the coupled inductor to design the High gain DC-DC boost converter. The construction of Core based on the parameters such as flux density, field intensity, permeability, flux leakages. In the last few years, there has been a growing interest in designing the interface dc–dc converters having the afore-mentioned features [13]. Although all kinds of dc–dc boost converters have been widely used in various FC applications, for charging a battery bank through an FC, a dc–dc buck–boost converter is required, provided that the output voltage is within the input voltage range [12]. Despite that, there are many single-active-switch buck–boost dc–dc converters such as Sepic, Cuk, and conventional inverting buck–boost and fly-back converters. The non-inverting buck–boost one constructed from combining boost and buck circuits in cascade with two separate controllable switches is in the choice for applications which are required in reducing stresses [4].

The high power magnetic components are mainly used in the defense and navigational applications, the efficient design of high power magnetic components increase the volume of power converter and reduce the size of converters with High efficiency and accuracy. It is used in automotive applications such as electric train, electric car, bike etc.. with ecofriendly[2]. The CCTT IM winding structure has less number of turns and having less internal capacitance. The low power loss material is selected to reduce the size as well as to increase the efficiency when combined with less turns windings which allows for a more compact design over more traditional IM design is optimized [1].

The loss is due to the conduction voltage drop, which can be minimized with the use of low on-drop power devices, such as thyristor or slow-speed insulated gate bipolar transistor (IGBT). In this version, IGBT is used in the unfolding circuit because it can be easily turned ON and OFF with gating control. Since only the boost dc–dc

* Research Scholar, St.Peter's University Chennai, TN, INDIA, *E-mail:* pmk.12345@gmail.com

** Professor & Director-Research, Syed Ammal Engineering College Ramanathapuram, TN, INDIA,*E-mail*:rdhanashekar@yahoo.com

*** PG Scholar, Syed Ammal Engineering College Ramanathapuram, TN,INDIA,*E-mail*: emfelava19@gmail.com

converter or buck dc–dc converter operates with high-frequency switching all the time in the proposed system, the efficiency is improved [3].

The two dc–dc converters analyzed and compared in this paper can be used for dc fast charging in EV/HEVs to extend the all-electric drive range. A municipal parking deck charging station with dc power distribution bus can employ a bidirectional dc–dc charger to allow vehicle-to-grid operation. Vehicle-to-grid applications operation can be useful in injecting real or reactive power to the grid to ensure current harmonic filtering or load balancing. A bidirectional converter with overlapping input–output voltage range would enhance the operational flexibility for vehicle-to-grid applications. [5]-[9]. The design such a converter for high power-density as well as high efficiency at light load is a challenging task. Regarding the main design concept, three main alternatives are:

1) High-power, single-phase design;
2) Multiphase design with interleaved modulation and phase shedding at low power;
3) Multiphase design with inductively coupled phases.

A single-phase, high power design is the least complex. However, compared to the other two approaches it cannot compete on power density and neither on low-power efficiency level due to bulky passives and unfavorable tradeoff in efficiency optimization for the high-power level [6], [14]-[17]. By increasing the turn's ratio of the coupled inductors which is similar to that in isolated converter, high-voltage conversion ratio is obtained. Unfortunately, the leakage inductor may have a great influence on the voltage stress of the switches [7]-[13].

Currently, large-scale PV systems interface to the grid via central or multi string inverter configurations presents the central inverter configuration, which is very commonly used due to its simplicity and low installation cost. The mismatch in power output from the limitation of single maximum power point tracking (MPPT), particularly under the change in irradiation conditions, and the power losses from the reverse-current blocking diodes degrade the efficiency of this PV configuration [8]. The high voltage conversion ratio is achieved by employing a coupled-inductor in the proposed bidirectional boost converter, which has the following features [10]-[15]:

1) The double-boost structure achieves a high voltage conversion ratio at the step-up or step-down stage;
2) Solitary control with signal in either the step-up or the step-down operating condition, an effectively simplified control circuit;
3) The leakage inductance energy of the coupled inductor is recycled, thus reducing the voltage stress on power switches;
4) To improve the efficiency of the system through the low on-drop switch.

2. CIRCUIT CONFIGURATION OF THE COVERTER MODEL

The circuit configuration of the proposed converter, which consists of four active switches S_1, S_2, S_3, S_4 and two sets of coupled inductor, four diodes D_1, D_2, D_3, D_4 and the output capacitor C_0.The simplified circuit model of the proposed converter is shown in Figure1.

3. DESIGN PARAMETERS

In the following electrical specifications are generated using the information provided in switching Period, T_s, Duty Cycle, D, Input Current in dc, I_{in}, Phase Current in dc, I_{phase}, Input Current Ripple, ΔI_{in}, Leakage Inductance, L_{lk}, Magnetizing Inductance, L_{mag}.

$$\text{Switching period} = T_S = \frac{1}{fs} \tag{1}$$

CIRCUIT DIAGRAM

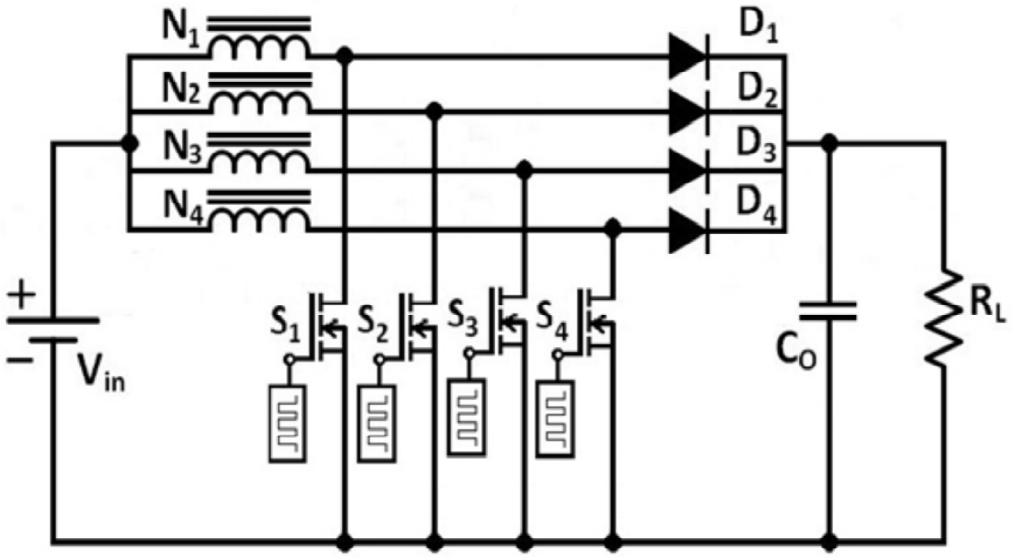

Figure 1: Circuit diagram of the Proposed Converter

$$\text{Duty cycle} = D = 1 - \frac{V_{in}}{V_{out}} \tag{2}$$

$$\text{Input current in } DC = I_{in} = \frac{P_{out}}{\eta_{conv} V_{in}} \tag{3}$$

$$\text{Phase current in } DC = I_{phase} = \frac{l_{in}}{2} \tag{4}$$

$$\text{Input current ripple } \Delta I_{in} = I_{in}\gamma_{in} \tag{5}$$

The leakage and magnetizing inductance values depend on whether the duty ratio is less than or greater than 0.5. The algorithm selects which equation is to be used, to calculate the leakage and magnetizing inductances, once the duty cycle is determined.

For $D < 0.5$;

$$L_{lk} \frac{V_{in}}{\Delta l_{in}} \left(\frac{D}{1-D} \right) (1-2D) T_s, \tag{6}$$

$$L_{mag} = 2L_{lk} \tag{7}$$

$$\Delta I_m = \frac{V_{in} T_s}{2L_{mag} + L_{lk}} \tag{8}$$

For $D > 0.5$;

$$L_{lk} = \frac{V_{in}}{\Delta l_{in}} (2D-1) T_s \tag{9}$$

$$L_{mag} = 2L_{lk} \tag{10}$$

$$\Delta I_m = \frac{V_{in} T_s}{2L_{mag} + L_{lk}} \tag{11}$$

The determines following, phase current ripple due to leakage inductance, $_{\Delta Iphase(lk)}$, phase current ripple, ΔI_{phase}, which is a combination of half the input current ripple and half of the magnetizing current ripple, peak phase current, $I_{phasemax}$

$$\Delta I_{phase(lk)} = \frac{\Delta I_{phase}}{2} \tag{12}$$

$$\Delta I_{phase} = \Delta I_{phase(lk)} + 0.5\Delta I_{mag} \tag{13}$$

$$\Delta I_m = I_{phase} + 0.5\Delta I_{phase} \tag{14}$$

4. CCTT IM CORE DIMENSIONS

The design and the structure of the core of the coupled inductor is shown in the Figure 2 and its dimensions are shown in the Table 1.

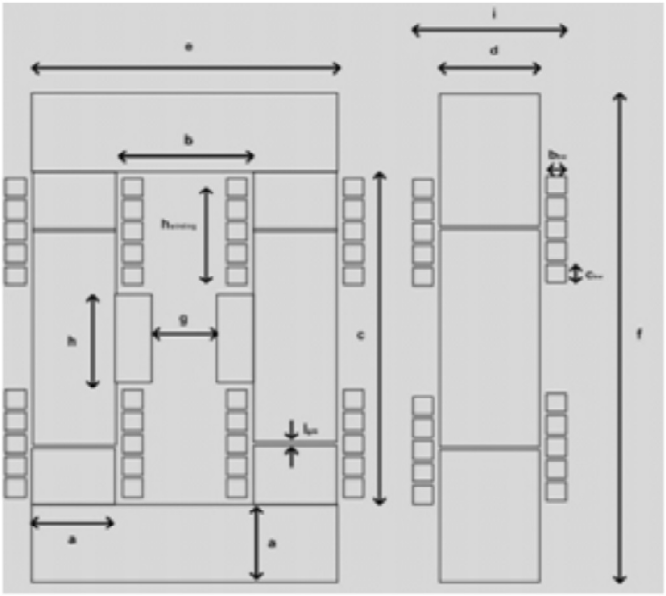

Figure 2: CCTT IM core dimensions

Table 1
CCTT IM core dimensions values

	Core Dimension		
Phase turns	N	–	8
Core width	a	mm	14
Window width	b	mm	21
Window height	c	mm	60
Core thickness	d	mm	16
Pole height	h	mm	20
Pole length	x	mm	9
Leakage gap	g	mm	3
Magnetizing gap	l_{g_mag}	mm	4*0.15
Winding width	b_{bw}	mm	18
Winding height	c_{bw}	mm	20

5. MAGNETIC MATERIALS

In this section, the CCTT IM structure is selected here with the variation in size to analyses the magnetic material, input frequency and ripple current, the power loss can be reduced through the temperature rise limitation and achieve more efficiency. The most optimum design is produced when all three constraints meet their limits. The tolerance level should be controlled to achieve the phase current imbalance issues, phase current imbalance in the magnetic core is similar to the magnetizing current flow the properties of the Magnetic material based on the flux density, field intensity values and the temperature coefficient depends on the material density are mentioned in below Table 2.

The magnetizing path air gap is divided in to many based on the rise in temperature and the temperature coefficient of the magnetic material is selected her is 70°c. The magnetic materials used in this analysis are ferrite

3C92 from Ferroxcube, iron-based amorphous metal 2605SA1 from Metglas and silicon steel 10JNHF600 from JFE. The structural parameters and material parameters and its specifications of different core windings are as in the Table 2 and Table 3.

Table 2
Properties of the Magnetic materials

	Magnetic Material Properties			
Material	2605SA1	10JNHF600	3C94	3C81
Magnetic Material Type	AM	SS	Ferrite	Ferrite
Manufacturer	Metglas	JFE	Ferroxcube	Ferrocube
Composition	Fe-B-Si	Fe-Si 6.5%	Mn-Zn	Mn-Zn
Saturation Flux density@70°C(T)	1.56	1.88	0.52	1.15
Relative Permiability (100°C@200kHz)	600	600	1800	2700
Curie Temparature (°C)	390	700	250	≥210
Thermal conductivity (W/mK)	10	18	3.5-5	≈1
Density	7.18	7.53	4.8	4.8
Core loss@0.1 T,100kHz(kW/m)	1380	1750	42	170

Table 3
Specification of CCTT IM Core

			CCTT IM and 2L Inductor Parameters	
Parameters	*Symbol*	*Units*	2L	CCTT IM
Input voltage	V_{in}	V	60	60
Output voltage	V_{out}	V	815	815
Input current	I_{in}	A	37	37.04
Phase current	I_{phase}	A	18	18.52
Input power	P_{in}	Kw	2.2	2.2
Frequency	f	kHz	45	45
Phase inductance	L_{phase}	µH	1645	–
Leakage inductance	L_{lk}	µH	–	5µ
Magnetizing inductance	L_m	µH	–	5µ
Input ripple	ΔI_{in}	A	2.20	2.8
Phase ripple	Δi_{phase}	A	4.15	14
			Core and Winding Mass and Volume	
Material	*Symbol*	*Units*	3C92	3C94
Core mass	M_c	kg	3.2	2.6
Leakage airgap	G	mm	–	3
Copper mass	M_{cu}	kg	0.56	0.56
Copper area	A_{cu}	mm²	52.2	52.2
Air gap per leg	I_g	mm	8×1.2	2×1.2
Core area	A_c	mm²	826	709
Turns	N	phase	8	8
Total boxed volume	V_{boxed}	cm³	642	574.18
Total mass	M_{total}	kg	3.45	3.16

6. HIGH-FLUX CCTT IM DESIGN

This section investigates the development of a low power CCTT IM using a laminated material 2605SA1 from Metglas. The use of ferrite 3C94 material allows for a increase in magnetic component size because of its relatively high saturation flux density in comparison to 2605SA1. The reduction in volume comes at the expense of increased core power loss and practical issues arise, such as the efficient removal of heat in an air cooled design, if the core power loss is too great. Therefore, it may be necessary to limit the specific core loss and temperature rise when designing a CCTT IM using a laminated material.

Figure 3(a) presents the variation in boxed volume for two 2605SA1 CCTT IM designs. The first design has no specific core loss and a temperature rise limit of 70°C. Conversely, the second design has a specific core loss limit of 160 kW/m3 and a temperature rise limit of 70°C. The 2L baseline and 3C94 CCTT IM boxed volume is included to give a complete pictureThe initial 2605SA1 CCTT IM design allows for a reduction in boxed volume of 35 % over the 3C94option but interestingly, when the design is constrained by specific core loss and temperature the boxed volume of the 3C94 option is very similar to that of the 2605SA1 CCTT IM.

Figure3(b) presents the total power loss for all of the designs. The initial 2605SA1 CCTT IM design has a power loss that is over 100 % greater than that of the 3C92 CCTT IM. The redesigned CCTT IM has a power loss that is 23 % less than the initial 2605SA1 option but it is still 40 % greater than that of the 3C94 CCTT IM.

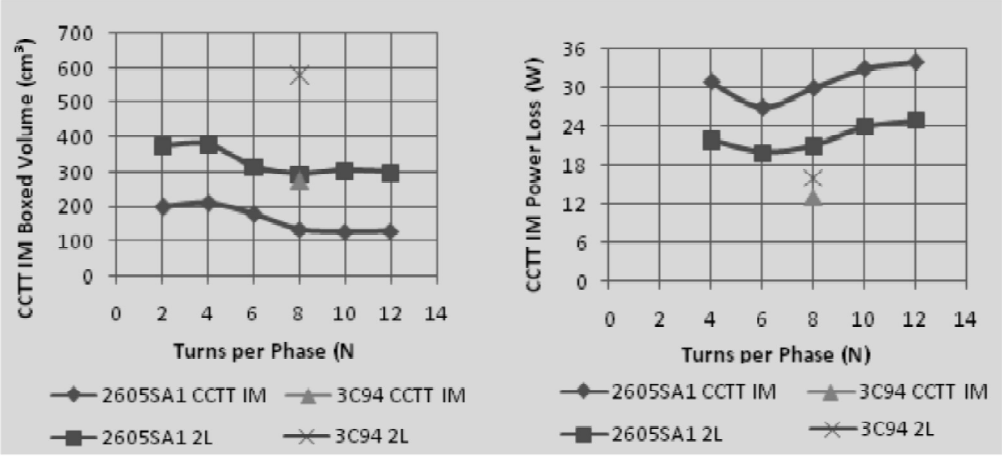

Figure 3: Variation in CCTT IM (a) boxed volume (b) power loss with turns per phase.

The initial 2605SA1 CCTT IM has a smaller air gap than the 3C94 CCTT IM while theredesigned 2605SA1 CCTT IM requires a larger air gap in order to produce the required leakage inductance. The above analysis indicates that the use of 2605SA1 allows for a reduction in boxed volume but this comes at the expense of excessive power loss and therefore, temperature rise. When a temperature rise limit is enforced, which would allow a practical design, the overall boxed volume significantly increases and the IM volume is greater than the 3C94 option. Thus, it is not realistic to use high flux density material at this low power level and frequency as its high saturation flux density capability is not being utilized.

7. OUTPUT OF THE DC- DC CONVERTER

The analysis of the output voltage and current in the converter (Figure 4) based on the material flux density and field intensity and are mentioned in the Figure 5 and distribution of flux in the material mentioned in the Figure 6.

The core winding and its turn's ratio which will differ the power output of the system by means of its leakage inductance and its power loss with respect to core leakage flux and field mentioned in the below Figure 7 and Figure 8.The ripple current analysis and saturation level is done through Figure 9.

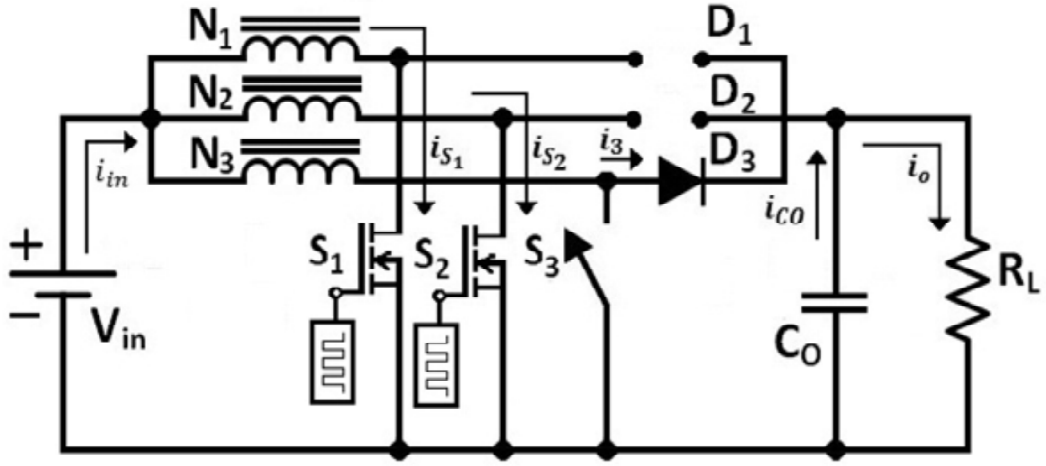

Figure 4: Waveform of Output voltage and Output current

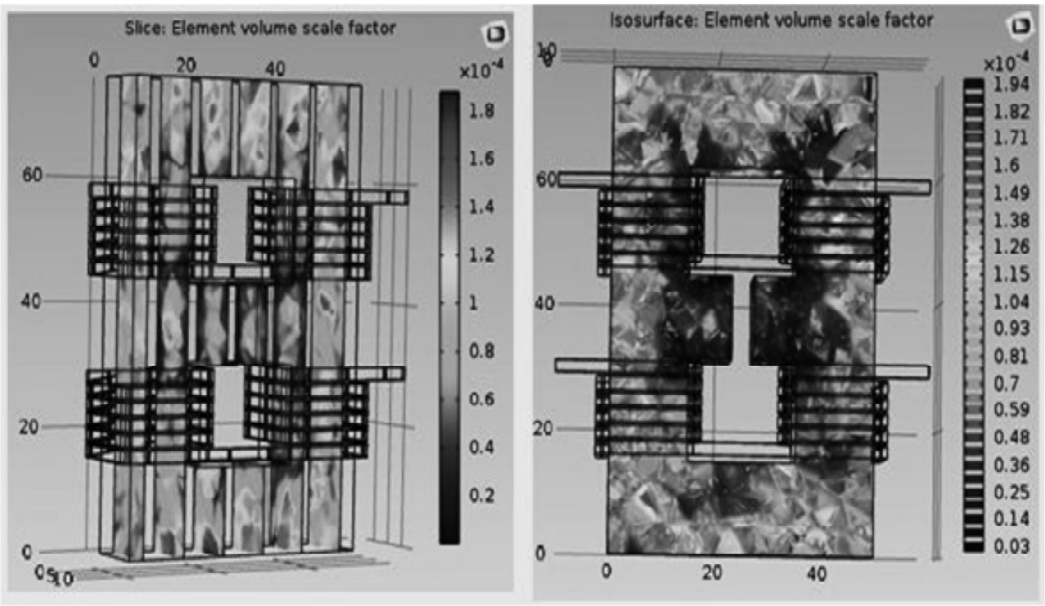

Figure 5: Flux distributed in the (a) Slice (b) Isosurface element volume of core CCTT IM 3C94

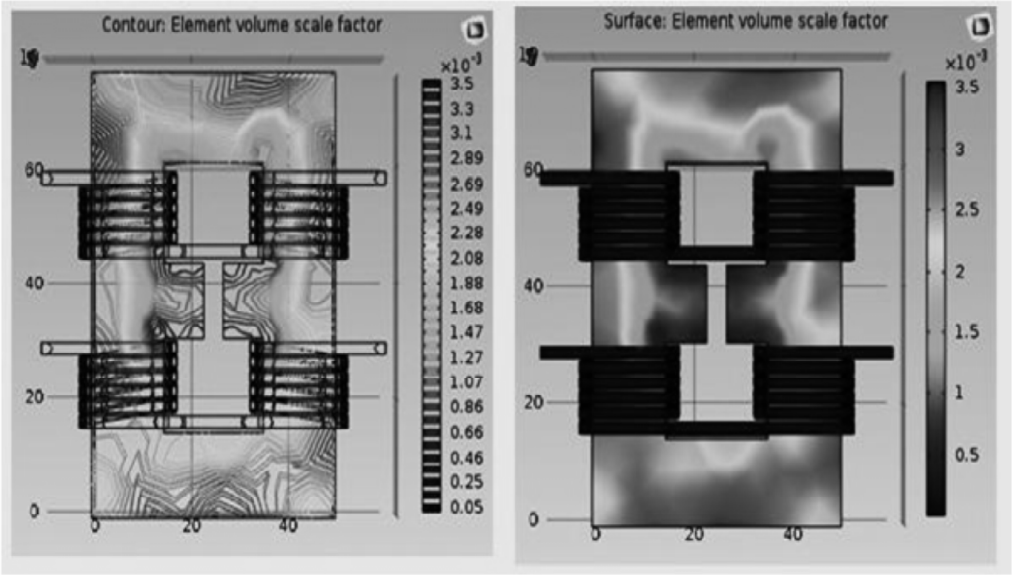

Figure 6: Flux distributed in the (a) contour (b) surface element volume of core CCTT IM 3C94

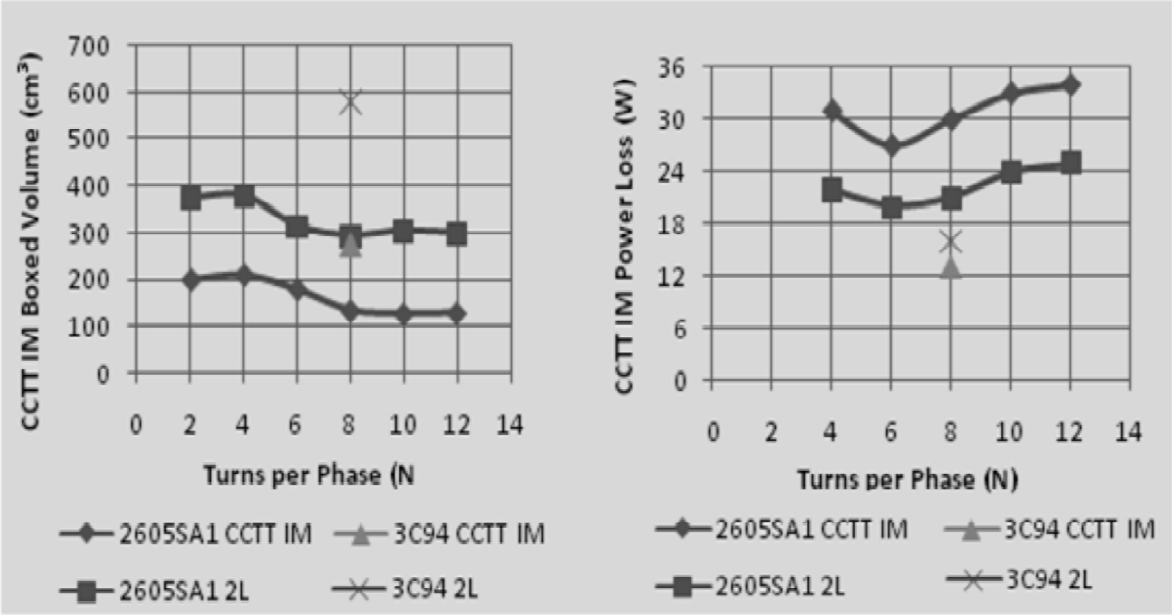

Figure 7: (a) Turns ratio with respect to boxed volume (b)Turns ratio with respect to power loss

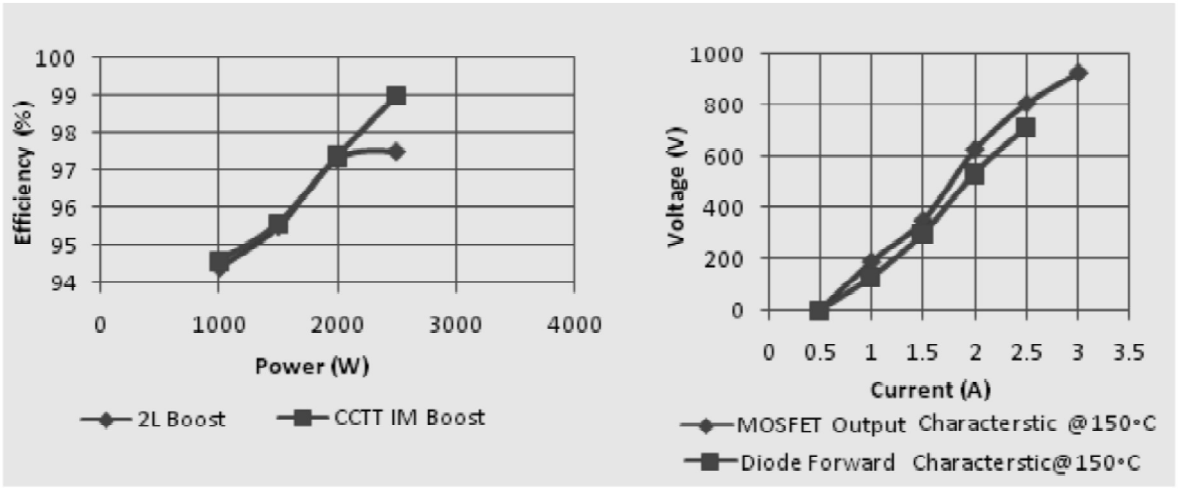

Figure 8: (a) Power ratings with respect to Efficiency (b) VI characteristics of switches

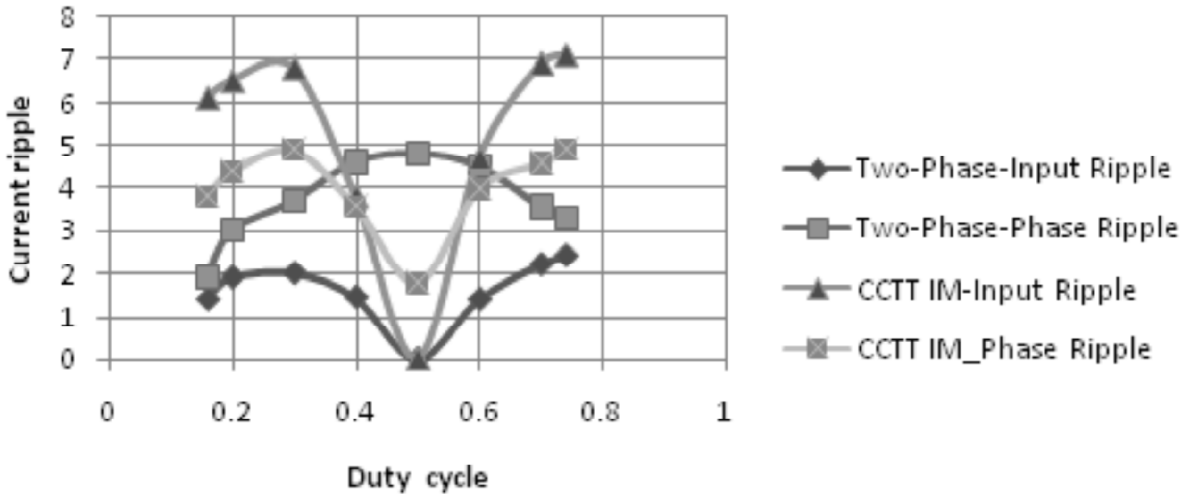

Figure 9: Ripple Current with respect to Duty cycle

The Hysteresis analysis of the flux density and field intensity of the magnetic material of different ferrite core and different winding structure with respect to the mutual and self-inductance phenomenon are concluded through the fallowing Figure 10.

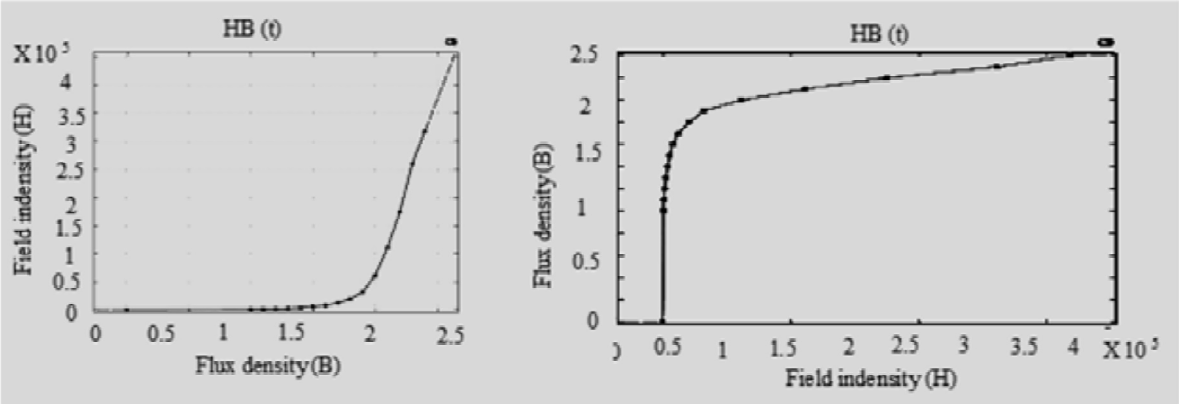

Figure 10: BH curve (a) forward (b) reverse

8. MAGNETIC FLUX PERFORMANCE ANALYSIS

The COMSOL Metaphysics software is widely used to analysis the materials properties. The materials properties are mentioned in Table 3, parts of materials shapes of CCTT IM core dimensions View, Magnetic flux density norm (T) Mesh in isosurface, Element volume scale factor of coil voltage in slice, Element volume scale factor in contour, Coil voltage (v) in slice, Magnetic flux density in top view surface, Magnetic flux density in all surfaces for CCTT IM 3C94 are designed and shown in the Figures 5, 6 and Table 3 in CCTT IM core dimensions values. The CCTT IM core dimensions View is showing in Table 1, the selected materials with its values and chosen the right materials for the coupled inductor circuit.

9. CONCLUSION

In two stages cascaded CCTT-core split with integrated magnetic structure of high gain DC-DC boost converter is useful for application of solar power operating system. The toroid magnetic components are applied in cascaded of two coupled inductor magnetic circuit along with good copper conductors, which are reduce the copper loss effects in the coupled inductor. The COMSOL Multiphysics software tool most suitable design of two stage coupled inductor components are designed with different structures are shown in above figures The CCTT IM design is displaying greater efficiency than the 2L model design and Magnetic poles are combined to support the shape and cover the leakage flux within the core window of the winding. The high gain DC-DC boost converter is simulated by PSIM software tool, which are produce the output power is 4.88 KW.

References

[1] Kevin J. Hartnett, John G. Hayes, Marek S. Rylko, Brendan J. Barryand Jerzy W. Maslon "Comparison of 8-kW CCTT IM and Discrete Inductor Interleaved Boost Converter for Renewable Energy Applications" IEEE Transactions on Industry Applications, Vol. 51, No. 3, pp. 2455-2469, May/June 2015.

[2] Kevin J. Hartnett, John G. Hayes, Michael G. Egan, and Marek S. Rylko, "CCTT-Core Split-Winding Integrated Magnetic for High-Power DC–DC Converters" IEEE Transactions on Power Electronics, Vol. 28, No. 11, pp. 4970-4984, November 2013.

[3] Zheng Zhao, Ming Xu, Qiaoliang Chen, Jih-Sheng (Jason) Lai, and Younghoon Cho, "Derivation, Analysis, and Implementation of a Boost–Buck Converter-Based High-Efficiency PV Inverter" IEEE Transactions on Power Electronics, Vol. 27, No. 3, pp. 1304-1313, March 2012.

[4] Vahid Samavatian and Ahmad Radan, "A High Efficiency Input/Output Magnetically Coupled Interleaved Buck–Boost Converter with Low Internal Oscillation for Fuel-Cell Applications: CCM Steady-State Analysis" IEEE Transactions on Industrial Electronics, Vol. 62, No. 9, pp. 5560-5568, September 2015.

[5] Mehnaz Akhter Khan, Adeeb Ahmed, Iqbal Husain, Yilmaz Sozer, and Mohamed Badawy, "Performance Analysis of Bidirectional DC–DC Converters for Electric Vehicles" IEEE Transactions on Industry Applications, Vol. 51, No. 4, pp. 3442-3452, July/August 2015.

[6] Martin Pavlovsky, Giuseppe Guidi, and Atsuo Kawamura, "Assessment of Coupled and Independent PhaseDesigns of Interleaved Multiphase Buck/Boost DC–DC Converter for EV Power Train" IEEE Transactions on Power Electronics, Vol. 29, No. 6, pp. 2693- 2704, June 2014.

[7] Yu Tang, Ting Wang, and Dongjin Fu, "Multicell Switched-Inductor/Switched-Capacitor Combined Active-Network Converters" IEEE Transactions on Power Electronics, Vol. 30, No. 4, pp. 2063-2072, April 2015.

[8] Hyuntae Choi, Mihai Ciobotaru, Minsoo Jang and Vassilios G. Agelidis, "Performance of Medium-Voltage DC-Bus PV System Architecture Utilizing High-Gain DC–DC Converter" IEEE Transactions on Sustainable Energy, Vol. 6, No. 2, pp. 464-473, April 2015.

[9] Yen-Shin Lai, Wei-Ting Lee, Yong-Kai Lin and Jian-Feng Tsai, "Integrated Inverter/Converter Circuit and Control Technique of Motor Drives with Dual-Mode Control for EV/HEV Applications" IEEE Transactions on Power Electronics, Vol. 29, No. 3, pp. 1358-1365, March 2014.

[10] Tsorng-Juu Liang, Hsiu-Hao Liang, Shih-Ming Chen, Jiann-Fuh Chen and Lung-Sheng Yang, "Analysis, Design, and Implementation of a Bidirectional Double-Boost DC–DC Converter" IEEE Transactions on Industry Applications, Vol. 50, No. 6, pp. 3955-3962, December 2014.

[11] Pritam Das, Majid Pahlevaninezhadand Amit Kumar Singh, "A Novel Load Adaptive ZVS Auxiliary Circuit for PWM Three-Level DC–DC Converters" IEEE Transactions on Power Electronics, Vol. 30, No. 4, pp. 2108- 2126, April 2015.

[12] Xiaoyong Ren, Xinbo Ruan, Hai Qian, Mingqiu Li and Qianhong Chen, "Three-Mode Dual-Frequency Two-Edge Modulation Scheme for Four-Switch Buck–Boost Converter" IEEE Transactions on Power Electronics, Vol. 24, No. 2, pp. 499-509, February 2009.

[13] K. I. Hwu and T. J. Peng, "A Novel Buck–Boost Converter Combining KY and Buck Converters" IEEE Transactions on Power Electronics, Vol. 27, No. 5, pp. 2236-2241, May 2012.

[14] P. Muthukrishnan and R. Dhanasekaran," Design and Simulation of Voltage Booster Circuit using Coupled Inductor", ARPN Journal of Engineering and Applied Sciences, Vol. 10, No. 6, pp. 2724-2729, April 2015.

[15] P. Muthukrishnan and R. Dhanasekaran," Performance and Analysis of Boost Converter with Capacitor Multiplier and Coupled Inductor for dc Applications", International Journal of Applied Engineering Research, Vol. 10, No. 6, pp. 5610-5615, 2015.

[16] P. Muthukrishnan and R. Dhanasekaran," Performance Evaluation of Closed loopBoost Converter using Coupled Inductor for drive Applications", International Journal of Applied Engineering Research, Vol. 10, No. 55, pp. 3392-3397, 2015.

[17. P. Muthukrishnan and R. Dhanasekaran," DC- DC Boost Converter for Solar Power Application", Journal of Theoretical and Applied Information Technology, Vol. 68, No. 3, pp. 630-636, October 2014.